Draft version December 21, 2016
Typeset using LaTeX **twocolumn** style in AASTeX61

THE FRB 121102 OBSERVING CAMPAIGN: MULTI-TELESCOPE RADIO BURST AND IMPLICATIONS FOR THE FRB POPULATION

C. J. Law,[1] G. C. Bower,[2] S. Burke-Spolaor,[3,4,5] B. J. Butler,[3] S. Chatterjee,[6] T. Cantwell,[7] S. H. Carey,[8] J. M. Cordes,[6] P. Demorest,[3] K. Grainge,[7] J. W. T. Hessels,[9,10] J. Hickish,[1,8] R. Fender,[11] T. J. W. Lazio,[12] D. Michilli,[9,10] M. A. McLaughlin,[4,5] K. Mooley,[11] Y. C. Perrott,[8] S. M. Ransom,[13] N. Razavi-Ghods,[8] M. Rupen,[14] A. Scaife,[7] P. Scott,[8] L. G. Spitler,[15] P. Scholz,[14] A. Seymour,[16,17] D. Titterington,[8] and R. S. Wharton[6]

[1] *Dept of Astronomy and Radio Astronomy Lab, University of California, Berkeley, CA 94720, USA*
[2] *Academia Sinica Institute of Astronomy and Astrophysics, 645 N. A'ohoku Place, Hilo, HI 96720, USA*
[3] *National Radio Astronomy Observatory, Socorro, NM 87801, USA*
[4] *Department of Physics and Astronomy, West Virginia University, Morgantown, WV 26506, USA*
[5] *Center for Gravitational Waves and Cosmology, West Virginia University, Chestnut Ridge Research Building, Morgantown, WV 26505*
[6] *Cornell Center for Astrophysics and Planetary Science and Department of Astronomy, Cornell University, Ithaca, NY 14853, USA*
[7] *University of Manchester, UK*
[8] *University of Cambridge, UK*
[9] *ASTRON, Netherlands Institute for Radio Astronomy, Postbus 2, 7990 AA, Dwingeloo, The Netherlands*
[10] *Anton Pannekoek Institute for Astronomy, University of Amsterdam, Science Park 904, 1098 XH Amsterdam, The Netherlands*
[11] *University of Oxford, UK*
[12] *Jet Propulsion Laboratory, California Institute of Technology, Pasadena, CA 91109, USA*
[13] *National Radio Astronomy Observatory, Charlottesville, VA 22903, USA*
[14] *National Research Council of Canada, Herzberg Astronomy and Astrophysics, Dominion Radio Astrophysical Observatory, P.O. Box 248, Penticton, BC V2A 6J9, Canada*
[15] *Max-Planck-Institut für Radioastronomie, Auf dem Hügel 69, D-53121 Bonn, Germany*
[16] *Arecibo Observatory, HC3 Box 53995, Arecibo, PR 00612, USA*
[17] *Max-Planck-Institut für Radioastronomie, Auf dem Hügel 69, Bonn, D-53121, Germany*

ABSTRACT

The millisecond radio transients known as Fast Radio Bursts have recently emerged as a mysterious, new class of astrophysical transient. The recent localization of FRB 121102 has helped identify its host galaxy, measure its distance, and infer intrinsic properties that comment on the broader FRB population. We present a detailed analysis of these bursts, including the first simultaneous detection of an FRB with multiple telescopes. We show that the burst spectra typically have a broad Gaussian shape on the scale of ~ 500 MHz with fine spectral structure consistent with either scintillation or unresolved intrinsic temporal structure. We present the burst energy distribution and temporal statistics for FRB 121102 and argue that the whole FRB population is adequately described by a single class similar to FRB 121102. We close with thoughts on optimal strategies to make new interferometric localizations of FRBs.

1. INTRODUCTION

Fast Radio Bursts (FRBs) are a new class of millisecond-duration radio transient with a dispersion measure (DM) that implies that they originate outside of our Galaxy. At extragalactic (and potentially cosmological) distances, they are not only unusually luminous, but they provide a new tracer of other galaxies and the intergalactic medium (IGM). In this way, FRBs have opened a whole new playground in astrophysics (e.g., Falcke & Rezzolla 2014; McQuinn 2014; Cordes & Wasserman 2016). However, that potential has been hamstrung by the lack of a definitive association of an FRB to an extragalactic host.

This paper is part of a series that presents the first localization and unambiguous identification of an FRB host (Chatterjee et al. 2017; Tendulkar et al. 2017; Marcote et al. 2017). FRB 121102, also known as the "repeating FRB", was first detected in November 2012 by the Arecibo Observatory (Spitler et al. 2014). In mid 2015, new Arecibo observations revealed a series of bursts at the same DM and sky position demonstrating that FRBs are capable of repetition (Spitler et al. 2016). Beginning in August of 2015, we made the first of nine detections of FRB 121102 with the Very Large Array (Chatterjee et al. 2017) and localized it to (RA, Dec) of (05h31m58.70s, +33d08m52.5s) with a precision of $0.1''$. Deep radio and optical observing shows that FRB 121102 is unambiguously associated with a persistent radio and optical source at a redshift of 0.193 (Tendulkar et al. 2017; Marcote et al. 2017).

FRB 121102 has now been localized four orders of magnitude better than any other FRB and placed at a cosmological distance. Its lookback and luminosity distances are 746 and 972 Mpc (Planck Collaboration et al. 2016), which are orders of magnitude larger than any other millisecond transient. This shows that FRBs are more energetic than any other millisecond radio transient, have a significant DM contribution from the IGM, and can be used to probe the IGM and their host galaxy. The promise implied by the first reported FRB (Lorimer et al. 2007) is now being realized.

The confirmation of a cosmological distance for FRB 121102 could have wide-ranging implications for the FRB population as a whole. However, it has not been demonstrated that FRB 121102 is representative of the overall FRB population. In fact, the repetition of its bursts is unique among all FRBs (Petroff et al. 2015), so it is natural to ask whether FRB 121102 is representative. An important first step is to demonstrate that the properties of FRB 121102 are consistent with the significant body of facts for the overall population (Macquart & Johnston 2015; Katz 2016). The repeating nature of FRB 121102 provides us with several statistical tests we can use to test this connection.

We can also assume that FRB 121102 is representative and use it to constrain the physical processes at play in the overall FRB population. In this case, we know that FRBs are apparently luminous, but it is not yet clear what processes are responsible. Possibilities include intrinsic processes, such as coherent, pulsar-like emission (Katz 2014; Luan & Goldreich 2014; Cordes & Wasserman 2016), or extrinsic effects like scintillation (Cordes et al. 2017). The simultaneous FRB 121102 observing campaign with the VLA, Arecibo, Effelsberg, GBT, and AMI-LA gives a more complete picture of the spectral structure of FRB radio emission. FRB repetition also has strong implications for calculations of their rate of occurrence (Connor et al. 2016) and comparison to other classes of transient, such as superluminous supernovae (Tendulkar et al. 2017).

Given that FRBs are now known to be useful probes of the IGM, there is even more motivation to make new detections and localizations. The relatively faint counterpart to FRB 121102 argues that direct localization of the radio burst will continue to be the best way to find optical hosts to measure distances. Our multi-telescope constraints on burst spectra, measurement of host properties, burst rate estimates, and other properties will inform new strategies for finding FRBs.

2. OBSERVATIONS

The data presented here were obtained from multiple programs and telescopes, but the central goal was to interferometrically localize FRB 121102 with the VLA. The observing strategy was to ensure simultaneous observing between the VLA and Arecibo observatories and add other observatories on a best-effort basis. We coordinated observing between the VLA, Arecibo, Effelsberg, and AMI-LA telescopes, as shown in Figure 1. Below, we summarize these observations, with a focus on those conducted simultaneously with VLA burst detections from FRB 121102.

2.1. *VLA*

The FRB 121102 observing campaign started in late 2015 with a 10 hr campaign observed at 1.4 GHz in the compact D configuration. In April through May 2016, we conducted a 40 hr campaign at 3 GHz in the C and CnB configurations in coordination with Arecibo. We concluded with a new, 40 hr, coordinated campaign from August through September 2016 in the B configuration and during the move to the most extended A configuration. In this last campaign, the first 34 hours of VLA observations were made at 3 GHz, while the last

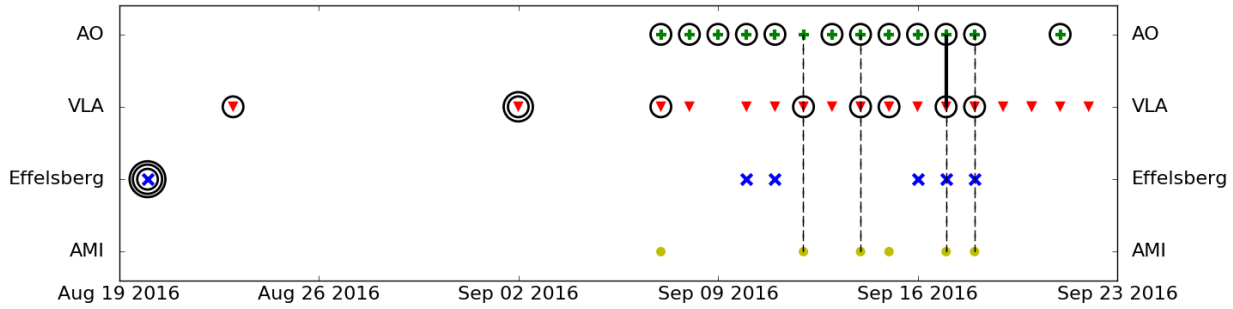

Figure 1. Summary of observing coverage and detections of FRB 121102 during the multi-telescope observing campaign in August and September 2016. Symbols show days with observations and circles highlight observations that detected bursts from FRB 121102. Multiple circles indicate multiple burst detections, except for Arecibo, which typically has multiple detections per observing session (a detailed analysis is left for a future paper). The black dashed lines show the VLA burst detections with simultaneous coverage at other telescopes. The solid black line shows the simultaneous burst detection at VLA and Arecibo.

6 hours were observed at 6 GHz. This paper focuses on the data collected at 3 GHz, which include all nine burst detections.

All VLA fast-sampled data were observed with 5 ms sampling, 256 channels, and dual-circular polarization (Law et al. 2015, as in). To maximize sensitivity, the channel frequency width was set to maintain sensitivity to the known DM of FRB 121102, while maximizing the total bandwidth. The total bandwidth at L (1.4 GHz), S (3 GHz), and C (6 GHz) bands was 256 MHz, 1024 MHz, and 2048 MHz, respectively. The 3 GHz data were recorded data in eight spectral windows with 32 channels each.

Observations in August and September were searched by a prototype version of *realfast*[1]. *realfast* is a real-time, fast imaging transient search system. The current prototype runs on existing, CPU-based hardware of the VLA correlator backend with transient search pipeline software called *rtpipe* (`https://github.com/caseyjlaw/rtpipe`; Law et al. 2015). Images were formed for each integration with a DM grid of 0, 546, 556.9, 560, and 565 pc cm^{-3} and a time resampling grid of 5, 10, 20, 40, and 80 ms. This DM grid was chosen to maintain 90% sensitivity to the nominal DM range of 554–560 pc cm^{-3}. Gain calibration is read from the "telcal" system, which uses phase-only calibration on the previous gain calibrator. A flux scale is calculated for each spectral window from an observation on xx (Bryan) and applied to all burst spectra.

Burst detections and localizations were made within hours of data being recorded. The transient search starts when data are recorded and proceeds slower than real-time, so we refer to it as "quasi real-time". For each trial DM, integration, and time scale, we form an image and calculate the S/N ratio for the peak pixel in the dirty image. Summary statistics are saved for images with S/N higher than 6.4, which captures the tail of the thermal noise distribution without adding significant computational or data volume burden. Each image with a pixel with S/N higher than 7.4 is relatively unlikely to be triggered by thermal noise in this configuration, so *realfast* generates a more detailed candidate visualization with an image and spectrum. More detailed analysis, including improved calibration and localization, is conducted offline.

Computational notebooks to reproduce the transient detection and localization can be found at `https://github.com/caseyjlaw/FRB121102`. Time cut-out visibility data are available at `https://doi.org/10.7910/DVN/TLDKXG`. Original visibility data are available under VLA program codes 16A-459 and 16A-496 and can be downloaded at `http://archive.nrao.edu`.

2.2. *Arecibo*

During the joint Arecibo-VLA campaign, Arecibo observed with the L-wide receiver using the PUPPI pulsar backend. The observational frequency range was 1.15 to 1.73 GHz and frequency resolution was 1.5625 MHz. We recorded total full Stokes polarization intensity spectra with time at a resolution of 10.24 μs. Each frequency channel was coherently dedispersed to 557 pc cm^{-3}, thereby eliminating intra-channel dispersion smearing. The ull width at half maximum (FWHM) beam size at band center is 3.3′.

In total, twelve Arecibo observations had some simultaneous coverage with the VLA. Four of those observations were simultaneous with bursts detected with the VLA and one of those observations detected the same VLA burst. During the first VLA burst with Arecibo

[1] See `http://realfast.io`.

coverage (MJD 57643), the PUPPI system failed so data were recorded with xx (Jason?) at C band. No detection was made in those Arecibo data. Overall, there were many more bursts detected at Arecibo than with the VLA and a more detailed analysis of those bursts will be presented in a future paper.

2.3. *Effelsberg*

Effelsberg observations were conducted with the S60mm receiver at an observing frequency of 4.6 to 5.1 GHz. Total intensity spectra were recorded by the PFFTS backend in pulsar search mode with a time resolution of 65.5 μs and 128 frequency channels. The system equivalent flux density is 18 Jy and a FWHM beam size of 2.4′at 4.85 GHz.

Five Effelsberg observations had some simultaneous coverage with the VLA, of which two were simultaneous with VLA bursts. Unfortunately, due to a configuration error, a 100 MHz bandwidth filter centered at 4.85 GHz was in place for both of these sessions. The sensitivity was about two times worse than the nominal value. No burst was detected in either observation.

2.4. *AMI*

We observed FRB 121102 with the Arcminute MicroKelvin Imager Large Array (AMI-LA; Zwart et al. 2008) for 3 hours each on four epochs starting at MJDs 57643, 57645, 57648, and 57649. Observations were made with the new digital correlator having 4096 channels across a 5 GHz bandwidth between 13–18 GHz with a 1 s integration time. The phase calibrator, J0518+3306, was observed every 12 minutes for about 1.5 minutes. The AMI-LA data were binned to eight 0.625 GHz channels and processed (RFI excision and calibration) with a fully-automated pipeline, AMI-REDUCE (e.g., Perrott et al. 2013). Daily measurements of 3C48 and 3C286 were used for the absolute flux calibration, which is good to about 10%.

We inspected the calibrated visibilities, and did not find any signal above 20 mJy in the 1s samples at and in the vicinity of the detected bursts. Concatenating and imaging the 12 hours of calibrated data with the CASA tasks *concat* and *clean* also does not yield any significant detection at the FRB location. Although the statistical 3σ upper limit is 60 μJy, extended mJy-level sources in the field cause sidelobe confusion (the AMI-LA angular resolution is $\sim 30''$), and the actual upper limit is larger. We introduced artificial point sources at the FRB location using the CASA *sm* tool, and found that these sources can be recovered as long as their peak flux densities are more than $\sim 100\mu$Jy. Hence, we place an upper limit of $100 \pm 10\mu$Jy on any quiescent or possible radio "afterglow" (on $\sim$days timescale) signal from the FRB. This limit is close to the flux density measured by the VLA (Chatterjee et al. 2017).

3. RESULTS

3.1. *Multi-Telescope Burst Spectrum*

Four of the VLA bursts were observed simultaneously with Arecibo and AMI-LA (Figure 1). Of these, the burst on 57648 was detected by Arecibo at the same time (after correcting for the known DM of FRB 121102). The Arecibo detection of this burst had a significance of xxσ (Jason).

Figure **to do** shows the dynamic spectrum formed from the phased VLA and Arecibo data... **Discuss dispersion correction, time alignment, chance of false association**

This simultaneous detection of a burst from roughly 1 to 4 GHz shows that some bursts emit over more than an octave of frequency. However, this is one of three VLA bursts with L-band coverage by Arecibo, which implies that those bursts had a smaller spectral width. However, all three VLA bursts with L-band Arecibo observations were relatively weak, so it is difficult to rule out L-band emission entirely. However, as described in §3.2.1, some of the VLA bursts appear to be fully contained in the band from 2.5 to 3.5 GHz, which implies a much smaller spectral coverage for typical bursts.

3.2. *VLA Bursts*

3.2.1. *Spectra*

Figure 2 shows the dynamic spectra of all nine bursts detected by the VLA. We improved on the initial analysis presented in Chatterjee et al. (2017) by using a better calibration scheme and optimizing the detection significance over a fine grid of DM (ΔDM = 1 pc cm^{-3}). Table 1 shows the improved burst parameters using this new scheme.

Figure 3 shows the spectrum of the integration and DM that maximizes the burst detection significance. After DM optimization, most bursts appear unresolved at the 5 ms time resolution of the VLA data. One exception is the brightest burst at 57633.68, for which roughly 10% of the peak flux density is seen in adjacent 5 ms integrations. **elaborate on 57633.68 time width**

The burst spectra are generally characterized by a broad, Gaussian shape with strong inter-channel modulation. We fit a Gaussian shape to each burst to estimate its characteristic width and peak flux (Table 1). The channel-scale modulation is as high as 100% (see §3.2.3) and is consistent with an exponential distribution. This introduces a strong bias to the best-fit Gaussian, but these simple fits are reliable enough to show that the typical burst has a spectral width of 500 MHz.

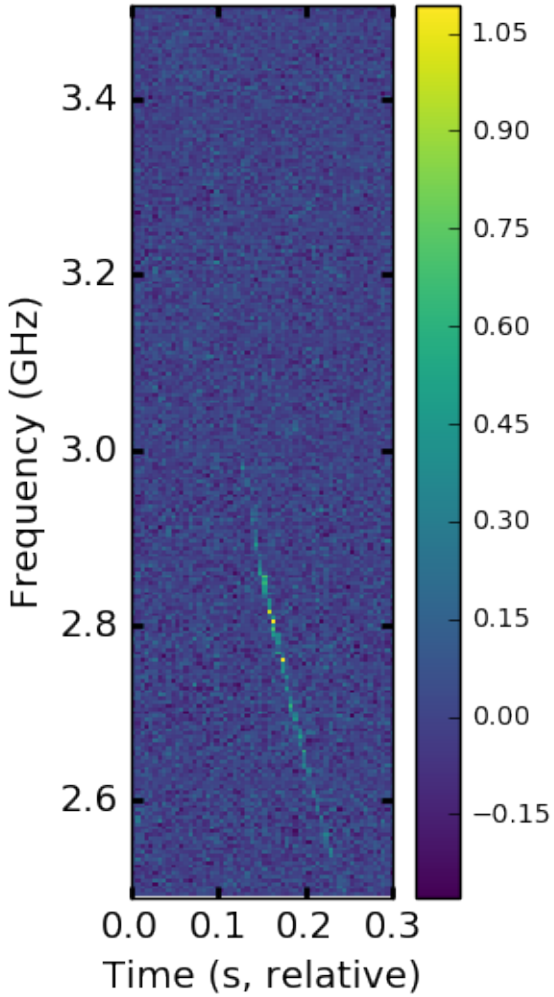

Figure 2. **Placeholder** Fill in with AO+VLA dynamic spectrum.

All but two of the best-fit Gaussians are centered inside the 3 GHz band and most appear contained by the 1 GHz wide band. This is consistent with previous detections of FRB 121102 by Arecibo, which showed quasi-broadband structure (Scholz et al. 2016) and large variation in the implied spectral index (Spitler et al. 2014). A detailed discussion of high-resolution FRB 121102 burst spectra seen by the Arecibo Observatory will be presented elsewhere (Hessels et al. 2017).

3.2.2. *Dispersion*

The initial VLA detections were made by searching a DM grid that allowed inter-DM sensitivity losses up to roughly 10% ($\Delta DM = 10$ pc cm^{-3} Cordes & McLaughlin 2003). In optimizing detection significance over a fine DM grid, we find optimal DM values range from 552 to 572 pc cm^{-3}. However, the uncertainty in the peak DM measurement is defined by the signal-to-noise of the burst and how this changes with DM.

Given that the apparent DM can potentially change due to intrinsic or extrinsic effects, we developed a more sophisticated system for modeling dispersion. We created a generative model to sample the likelihood distribution as a function of DM (Hogg et al. 2010). We use the Gaussian shape (see §3.2.1) along the spectral axis and apply a frequency-dependent delay for a given dispersion model. The likelihood is directly sampled by calculating the product of probabilities on a per-pixel basis of the 2-dimensional dynamic spectrum. Uncertainties in each pixel are drawn from a uniform Gaussian error distribution that is estimated from the data.

Figure 4 compares the 95% confidence intervals on the DM for all nine VLA bursts to the range of DM previous observed (Spitler et al. 2014; Scholz et al. 2016). The DM confidence intervals are not consistent with each other or a single DM. This suggests that there are apparent DM changes between bursts, either due to intrinsic burst structure or actual changes to the DM col-

Table 1. Properties of Bursts from FRB 121102

Date (MJD)	S_{int} (mJy)	Image S/N	E_{int} (10^{38} erg)	DM_{opt} (pc cm^{-3})	S_{peak} (Jy)	Center (GHz)	FWHM (MHz)
57623	258	38	7.1	561	0.41	2.8	300
57633.68	2000	179	56	554	1.89	3.1	520
57633.70[a]	105	15	5.5	559	>0.28	<2.5	>350
57638	65	12	1.7	556	0.07	3.1	430
57643	375	100	11	560	0.39	2.8	530
57645	38	13	1.0	572	0.05	2.8	350
57646[a]	69	20	3.4	555	>0.16	<2.5	>380
57648[b]	97	25	2.6	559	0.11	2.8	420
57649	110	36	3.7	552	0.07	2.9	870

[a] Best-fit Gaussian is not centered in 3 GHz band, so spectral parameters are limits.

[b] Detected simultaneously with Arecibo between 1.15 and 1.73 GHz.

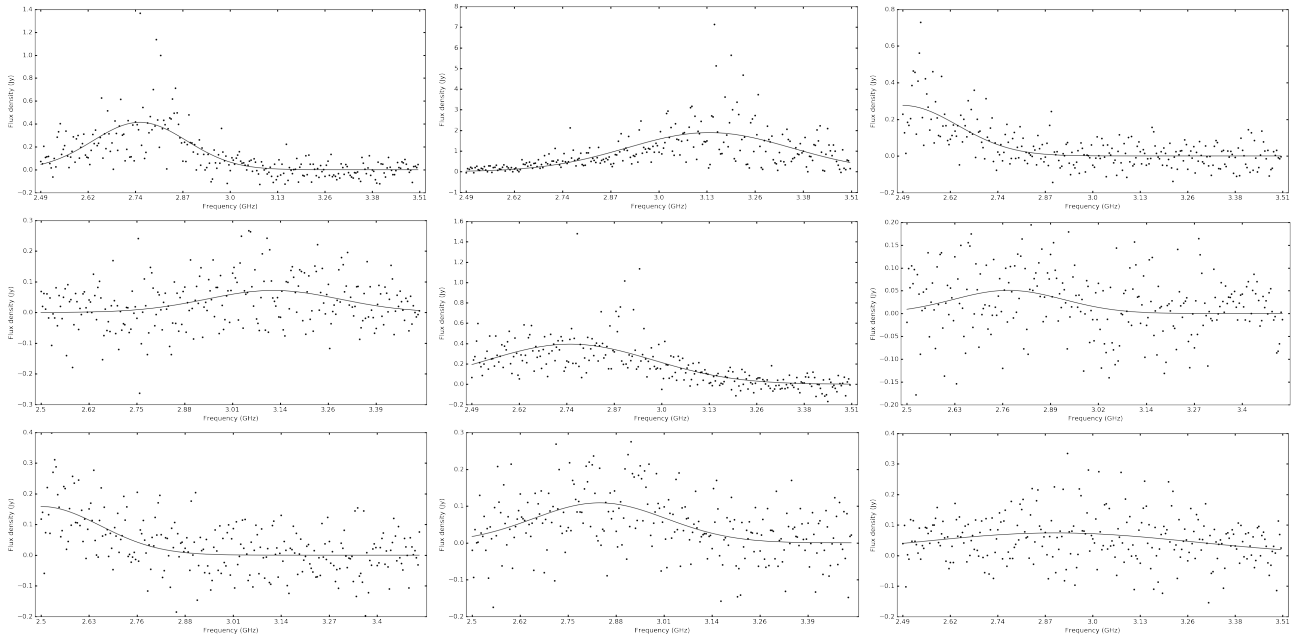

Figure 3. Spectra of nine bursts seen by the VLA from 2.5 to 3.5 GHz. Starting at the top left (moving right and then down), they correspond to bursts on MJDs 57623, 57633.68, 57633.70, 57638, 57643, 57645, 57646, 57648, and 57649. Note that bursts are detected in 5 ms images generated from dedispersed visibilities. The solid line is a best-fit Gaussian model derived from spectra binned by a factor of 4.

umn density. Elsewhere, we present high-resolution dynamic spectra at 1.4 GHz that show how intrinsic spectral structure can bias the apparent DM of individual bursts (Hessels et al. 2017). The FRB emission process has not yet been defined, so it is not clear how the intrinsic structure can bias DM as a function of frequency.

3.2.3. *Spectral Autocorrelation*

Autocorrelation of the burst signal (both temporal and spectral) can be used to infer both intrinsic properties and modulation due to scintillation (Cordes et al. 2017). Figure 5 shows the spectral autocorrellation for the strongest burst (MJD 57633.68). The is no strong excess correlation near the channel resolution, which limits the correlation width to less than roughly 4 MHz. This is broadly consistent with expectations of Galactic diffractive scintillation bandwidth (3–9 MHz near 3 GHz Cordes & Lazio 2002).

3.2.4. *Circular Polarization*

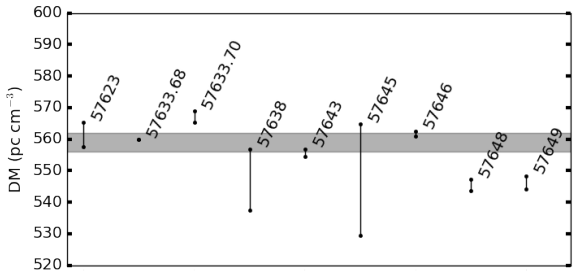

Figure 4. DM 95% confidence intervals of the nine 3 GHz bursts detected by the VLA. The grey band shows the range of DM previously detected at 1.4 GHz (± 3 pc cm^{-3}).

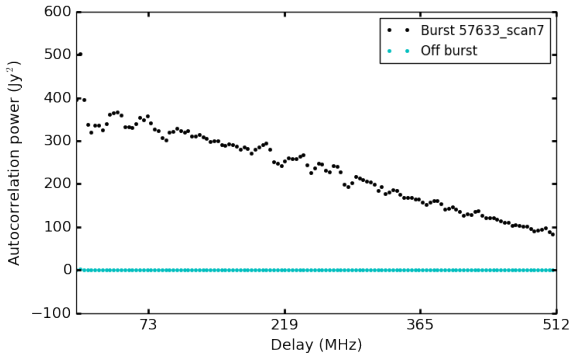

Figure 5. The spectral autocorrelation as a function of frequency for the burst from FRB 121102 at MJD 57633.68. Black dots show the autocorrelation for the burst and cyan shows the autocorrelation of a representative spectrum with no burst.

The VLA S-band recievers natively measure circular polarization, although for observing efficiency we chose not include polarization calibration procedures. Crude constraints on circular polarization are possible by comparing the burst intensity in right and left-hand polarized data products. The apparent circular polarization fraction ($(RR-LL)/(RR+LL)$) for the most significant bursts are all less than 3%. FRB 121102 was located $2.3'$away from pointing center, where systematic effects have been measured as large as 3% (Perley et al 2016, VLA memo). Given that systematic effects dominate the apparent circular polarization, we conclude that the true fractional circular polarization is less than 3%.

3.3. *Temporal Statistics*

Burst detections were made very inhomogenously through the larger (63 hours) observing campaign of FRB 121102. In the first 30 hours of observing at S-band no bursts were detected, while nine bursts were detected in the last 27 hours of S-band observing. The data quality is high, so the inhomogeneous burst distribution shows that the burst detection probability was not stationary. Assuming that the burst detection probability follows a Poisson distribution, the nondetection in the first half of S-band limits the FRB rate to R < 0.1 hour^{-1} (95% confidence limit). The mean detection rate for the last part of the campaign was R $= 0.3$ hour^{-1}.

There is weak evidence that the FRB 121102 burst rate changed during the last 27 hours of the S-band campaign. We modeled the event detection probability as a Poisson probability function, $P_i(\lambda)$, with rate parameter that evolves linearly in time relative to the first VLA burst $\lambda = a + b(\mathrm{MJD_i} - 57623)$. By directly sampling the joint probability distribution, $\prod_i P_i$, we can exclude a constant rate with $\sim$85% confidence. This weak constraint is consistent with the broader trend seen by the VLA and Arecibo.

During the August–September 2016 observing campaign, the typical observation lasted about two hours and was sampled with a 5 ms cadence. We used the Lomb-Scargle periodogram (Scargle 1982) to search for periodic structure over a wide range of timescales. The time series is calculated by binning the burst detection rate per 100 ms (Palliyaguru et al. 2011, always either 0 or 1, see also). The spectral power calculated for periods between 0.8 and 80 s shows no power in excess of the typical 95% confidence bound estimated from shuffled data. We verified that simulating nine bursts drawn from a simple rotational model would produce excess power using this approach. However, it is difficult to put strong constraints on more complex rotational models (e.g., with wide pulse phase windows or glitches Camilo et al. 2007; Archibald et al. 2013)

3.4. *Energy and Brightness Distribution*

Knowing the burst distance, we calculate their total energy by integrating flux in time and frequency (Table 1). The VLA has also shown for the first time that many bursts are contained within the 3 GHz band. For those bursts, the mean S-band flux density can be converted to an energy with no assumptions about its spectral properties.

This uniform sample of burst energies can be used to infer more general properties of FRB 121102. We treat the detection probability as a Poisson process with a rate that scales with the energy as a powerlaw. Figure 6 shows the probability distribution for the powerlaw amplitude and index for the sample of nine VLA bursts. The energy powerlaw index 1σ bounds range from –0.5 to +0.4; for a cumulative energy distribution, this corresponds to a powerlaw index of roughly –0.6. The flatness of the distribution is also clear from range of significance of the nine bursts (12 to 179σ). All bursts are much brighter than the sensitivity limit, so the distribution

is not affected by a completeness limit. **elaborate on limit and completeness**

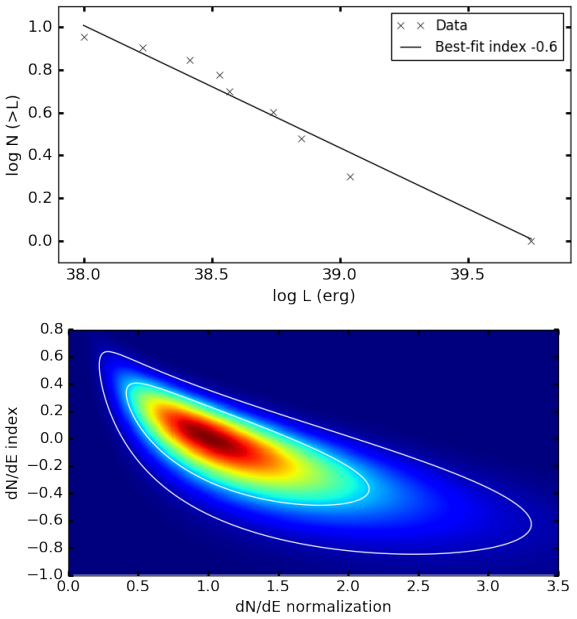

Figure 6. *Top:* Cumulative energy distribution with powerlaw fit for the nine VLA bursts from FRB 121102. *Bottom:* Probability distribution of energy model of the differential luminisotiy distribution. The powerlaw is referenced to $L = 2 \times 10^{38}$ erg.

Assuming that FRB 121102 is representative of the overall FRB population, we can use the energy distribution of the former to infer properties of the latter. The primary observable of the FRB population is the flux distribution. We use a Monte-Carlo technique to simulate an FRB population with a given energy/luminosity and spatial distribution. To reproduce the observed FRB sample, we select the brightest N bursts and fit their fluxes with a powerlaw. The tail of this distribution selects for extrema, such cut-offs in the intrinsic distribution or propagation effects (Macquart & Johnston 2015; Cordes et al. 2017). Therefore, we sample 100 such populations and measure 95% bounds on the distribution of cumulative flux distribution index.

These simulations confirm previous work that shows that in many circumstances the cumulative flux distribution follows a Euclidean distribution (index $= -1.5$; Lyutikov et al. 2016). To reproduce the flatness (index ≈ -1) of the observed flux distribution, we need to incorporate other effects. **in progress** (new figure?)

4. DISCUSSION

4.1. *Emission Physics and Burst Energetics*

The measurement of a redshift to the host of FRB 121102 allows us to measure the burst luminosity and energy. We now know that FRB 121102 is detectable with the VLA out to $z = 0.7$ and much farther with Arecibo. This confirms the results presented in Chatterjee et al. (2017), which quoted a energy on the order of 10^{38} erg. The more refined analysis presented here results in somewhat higher burst fluxes, so the brightest VLA burst energy ranges as high as 5×10^{39} erg.

However, the total energy emitted by FRB 121102 can be orders of magnitude different than this isotropic, apparent energy. While the emission process is not yet known, it is neccessarily coherent (Spitler et al. 2016; Hessels et al. 2017), so relativistical beaming will amplify the apparent brightness. Propagation effects (e.g., scintillation, scattering) can also modify the radio signal in a variety of ways (Cordes et al. 2017) and the duration of the emission in the source frame is not known. In any case, the energy scale is still larger than any Galactic class of fast radio transient and requires either a new process or dramatic scaling of known emission processes (Lyutikov et al. 2016; Cordes & Wasserman 2016).

4.2. *FRB Flux Distribution*

Doubts were cast on the first FRB detection ("Lorimer burst") due to its unusually high brightness. The lack of lower-significance detections suggested that this burst was unlikely to be part of any astrophysical population. With more detections, it has become clear that the FRB population has a relatively flat flux distribution (Vedantham et al. 2016; Li et al. 2016; Lawrence et al. 2016). This fact was recently demonstrated by yet another detection of an extremely bright FRB (Ravi et al. 2016).

Discussion of energy/flux distribution analysis presented in §3.4)

It is not yet clear whether FRB 121102 can be treated as a representative of the broader FRB population. Spitler et al. (2016) describes burst spectral structure that is intrinsic, or at least dominated by propagation effects close to the emitting region. On the other hand, (Cordes et al. 2017) have identified a variety of propagation effects in our own Galaxy that can plausibly modify the observed brightness distribution.

4.3. *Repetition*

The burst rate analysis presented in §3.3 shows that the detection probability of FRB 121102 is not stationary. As mentioned above, this could be caused by intrinsic events (e.g., magnetar outburst) or propagation effects. While a detailed analysis of temporal correlation will require more bursts and/or more sophistication, it is clear that FRB 121102 has significant correlation on

short timescales (sometimes called a "red spectrum"; Connor et al. 2016). Another way of stating this is that the detection of a burst improves odds of finding more bursts in near-future observations.

If this statistical property describes other FRBs, it weakens previous constraints on repetition (Petroff et al. 2015; Law et al. 2015). It is possible that other FRBs have repeating bursts, although calculating a limit requires knowing the temporal correlation function that defines the repetition. Repetition also implies that there are fewer phyiscal sources of FRBs than implied by the burst detection rate.

4.4. *FRB Rate*

Sarah: can you update this as a per-SFR rate? Assuming that FRB 121102 is from the same population as the other FRBs, the measurement of a distance for the host of FRB 121102 allows us to re-evaluate the cosmic volume and event rate per galaxy for the FRB population. The estimated projected FRB rate R_p understates the true rate by a beaming fraction Ω_b ($\sim$10%; Tauris & Manchester 1998). For a comoving volume $V(z)$ and galaxy number density $\Phi(M)$, the rate per galaxy is $R_{FRB} = R_p/(\Omega_b \Phi(M) V(z))$.

The first such rate estimate was made by Thornton et al. (2013), who used the measured DM to estimate a characteristic distance for their sample of 4 FRBs. They assumed that all of the extragalactic component of the DM was caused by the IGM and scaled as $DM \approx z \times 1200\mathrm{pc\ cm^{-3}}$ (Ioka 2003; Inoue 2004). They also calculated the number of galaxies by assuming a characteristic L_* galaxy (corresponding to stellar mass $M_* \approx 1011M$; Baldry et al. 2012).

Our calculation differs in that we have better estimates of all three parameters. First, the projected FRB rate is now believed to be closer to $2\times10^3\ \mathrm{sky^{-1}day^{-1}}$ at high Galactic latitudes and flux densities brighter than 1 Jy ms (Lawrence et al. 2016; Champion et al. 2016; Rane et al. 2016). FRB 121102 is associated with a relatively small galaxy (5×10^7 Msun), which are roughly a factor of 100 more abundant ($\Phi(M) \approx 10^{-2}\mathrm{Mpc^{-3}}$; Faber et al. 2007). Finally, the measured distance for FRB 121102 suggests that the extragalactic DM has comparable contributions from the IGM and host galaxy.

This reduces the characteristic distance by a factor of two and the volume by an order of magnitude. Considering these factors, we assume a characteristic redshift of the population that is twice that of FRB 121102 to estimate $R_{FRB} \approx 10^{-4}(0.1/\Omega_b)\mathrm{galaxy^{-1}year^{-1}}$, which is two orders of magnitude lower than previously estimated (Thornton et al. 2013, assuming isotropic radiation;).

There are significant caveats to the comparison of this rate to the rates of other classes of transient. This isotropic FRB rate assumes a projected FRB rate at a single (observationally defined) flux limit and that no bursts repeat. Using this calculation with data from more sensitive telescopes, we might infer a higher rate. However, if we assume that FRB 121102 is representative of the overall FRB population, then more sensitive observations would be more likely to find repeating FRBs that would effectively depress the estimate of the underlying isotropic rate per source. In this model, these two effects partially cancel, although without a physical model it is difficult to say how well.

4.5. *Observing Strategies*

As discussed above, Connor et al. (2016) note that the FRB repetition implies that the number of FRB-generating sources is smaller than implied by the number of bursts. In some scenarios, this means that there are areas on the sky that may contain no FRBs. Wide, shallow surveys are the preferred strategy for blind detection of FRBs. However, future efforts to localize FRBs are still most likely to succeed by targeting known FRBs to catch repetitions, assuming that all FRBs repeat. Finally, we note that the average spectral coverage of bursts from FRB 121102 are relatively narrow ($<$ 1 GHz) and the coverage changes dramatically between bursts. Thus, the odds of detecting a burst will improve linearly with bandwidth for bandwidths wider than this characteristic scale.

5. CONCLUSIONS

Prior to being established as a cosmological source, the low Galactic latitude of FRB 121102 made it a somewhat compromised member of the FRB class. With its cosmological distance firmly established, FRB 121102 now serves as a new kind of standard by which FRBs are defined. That fact, combined with an abundance of data collected during its high activity state, allows us to think more generally about the physics of broader FRB population.

We presented the first multi-telescope detection (Arecibo and VLA) of an FRB. By detecting this burst from 1.2 to 4.5 GHz, we have demonstrated that some bursts have broad spectral structure. However, three other VLA bursts are undetected by Arecibo. That, combined with the measurement of spectra within the VLA band, suggest that the typical burst has a characteristic Gaussian spectral shape with width $\sim$ 500 MHz.

Flux/lum distribution

Analysis of the VLA burst times shows that the burst rate is highly variable. This shows that past constraints

on FRB repetition are weaker than previously inferred. The combination of relatively narrow spectral structure, flat energy and flux distributions, and variable burst rate suggests that repeated observations, wide bandwidth, and large instantaneous field of view all improve the chance of detection.

New, arcsecond-scale localizations will continue to be highly informative, given that FRB hosts may be faint and can confuse the inference of a properties of the intergalactic medium (Deng & Zhang 2014). FRB 121102 was localized within hours by a prototype version of *realfast*, but an expanded *realfast* system is now under construction. This platform will search a TB/hour data stream in real time in parallel with ongoing VLA observations, potentially detecting and localizing multiple FRBs per year. Sarah: any refinement to this statement?

ACKNOWLEDGEMENTS

The National Radio Astronomy Observatory is a facility of the National Science Foundation operated under cooperative agreement by Associated Universities, Inc.. This project was supported by the University of California Office of the President under Lab Fees Research Program Award 237863. MAM is supported by NSF award #1458952. This research made use of Astropy, a community-developed core Python package for Astronomy (Astropy Collaboration, 2013).

REFERENCES

Archibald, R. F., et al. 2013, Nature, 497, 591

Baldry, I. K., et al. 2012, MNRAS, 421, 621

Camilo, F., et al. 2007, ApJ, 663, 497

Champion, D. J., et al. 2016, MNRAS, 460, L30

Chatterjee et al. 2017, Nature

Connor, L., Pen, U.-L., & Oppermann, N. 2016, MNRAS, 458, L89

Cordes, J. M., & Lazio, T. J. W. 2002, ArXiv Astrophysics e-prints

Cordes, J. M., & McLaughlin, M. A. 2003, ApJ, 596, 1142

Cordes, J. M., & Wasserman, I. 2016, MNRAS, 457, 232

Cordes et al. 2017, in prep

Deng, W., & Zhang, B. 2014, ApJL, 783, L35

Faber, S. M., et al. 2007, ApJ, 665, 265

Falcke, H., & Rezzolla, L. 2014, A&A, 562, A137

Hessels et al. 2017, in prep

Hogg, D. W., Bovy, J., & Lang, D. 2010, ArXiv e-prints

Inoue, S. 2004, MNRAS, 348, 999

Ioka, K. 2003, ApJL, 598, L79

Katz, J. I. 2014, PhRvD, 89, 103009

—. 2016, Modern Physics Letters A, 31, 1630013

Law, C. J., et al. 2015, ApJ, 807, 16

Lawrence, E., Vander Wiel, S., Law, C. J., Burke Spolaor, S., & Bower, G. C. 2016, ArXiv e-prints

Li, L., Huang, Y., Zhang, Z., Li, D., & Li, B. 2016, ArXiv e-prints

Lorimer, D. R., Bailes, M., McLaughlin, M. A., Narkevic, D. J., & Crawford, F. 2007, Science, 318, 777

Luan, J., & Goldreich, P. 2014, ApJL, 785, L26

Lyutikov, M., Burzawa, L., & Popov, S. B. 2016, MNRAS, 462, 941

Macquart, J.-P., & Johnston, S. 2015, MNRAS, 451, 3278

Marcote et al. 2017, ApJL

McQuinn, M. 2014, ApJL, 780, L33

Palliyaguru, N. T., et al. 2011, MNRAS, 417, 1871

Perrott, Y. C., et al. 2013, MNRAS, 429, 3330

Petroff, E., et al. 2015, MNRAS, 454, 457

Planck Collaboration et al. 2016, A&A, 594, A13

Rane, A., Lorimer, D. R., Bates, S. D., McMann, N., McLaughlin, M. A., & Rajwade, K. 2016, MNRAS, 455, 2207

Ravi, V., et al. 2016, ArXiv e-prints

Scargle, J. D. 1982, ApJ, 263, 835

Scholz, P., et al. 2016, ArXiv e-prints

Spitler, L. G., et al. 2014, ApJ, 790, 101

—. 2016, Nature, 531, 202

Tauris, T. M., & Manchester, R. N. 1998, MNRAS, 298, 625

Tendulkar et al. 2017, ApJL

Thornton, D., et al. 2013, Science, 341, 53

Vedantham, H. K., Ravi, V., Hallinan, G., & Shannon, R. M. 2016, ApJ, 830, 75